

Research papers

Semi-analytical model for pumping tests in discretely fractured aquifers

Lei Wang ^{a,b}, Hong Zhou ^{a,b}, Junlei Wang ^c, Rongze Yu ^c, Jianchao Cai ^{d,*}^a Key Laboratory of Theory and Technology of Petroleum Exploration and Development in Hubei Province, China University of Geosciences, Wuhan 430074, China^b Key Laboratory of Tectonics and Petroleum Resources (Ministry of Education), China University of Geosciences, Wuhan 430074, China^c PetroChina Research Institute of Petroleum Exploration and Development, Beijing 100083, China^d Institute of Geophysics and Geomatics, China University of Geosciences, Wuhan 430074, China

ARTICLE INFO

This manuscript was handled by Corrado Corradi, Editor-in-Chief, with the assistance of Mohsen M. Sheriff, Associate Editor

Keywords:

Semi-analytical model
Pumping tests
Discretely fractured aquifers
Wellbore drawdown

ABSTRACT

In this paper, a novel semi-analytical model for pumping tests in discretely fractured aquifers with randomly distributed and finitely conductive fractures is presented to investigate the wellbore drawdown transient behaviour. An aquifer model and discrete fracture model are established. The flux and drawdown equivalent conditions in the Laplace space are applied in the fracture wall to couple the fluid flow in both systems. The advantage of the proposed semi-analytical model is that only fractures must be separated into segments, not the entire domain. Then, a matrix of the fracture segment in Laplace space can be built and solved by using Gauss's elimination method. A final solution for wellbore drawdown can be easily evaluated using the numerical Laplace inversion algorithm of Stehfest. The model is compared with a previous result of an extended well. The proposed model allows us to consider the problems of pumping tests in complex fracture networks, including parallel uncrossed fracture networks, arbitrary distribution non-intersected fracture networks, and intersected fracture networks with isolated fractures. In the past studies, some scholars have found that the drawdown or pressure derivative curve will present only one dip valley which looks like a V-shaped curve for the naturally fractured confined aquifer or reservoirs, and number of dip valleys are only related to porous media type. However, this study illustrates that the drawdown transient behaviour and the number of dip valleys are closely related to fracture density, fracture conductivity, fracture length, fracture orientation, fracture distribution, position of a pumping well, and the distance between the pumping well and fracture.

1. Introduction

Fractured aquifers play an important role in regional water supplies. Many fractures can exist in carbonate, sandstone, volcanic, and other hard rock formations (Gerke and van Genuchten, 1993). The widely known double porosity model is often used to study the unsteady behaviour of drawdowns (Warren and Root, 1963). A previous study noted that the spatial arbitrary unit is composed of a matrix and fracture, the matrix's main role is to store fluid, and the fracture acts as the flow channel for the fluid (Smedt, 2011). The exchange function is often used to describe the inter-porosity flow between the matrix and fracture (Kazemi, 1969).

The assumption of a continuous medium was used to define double porosity models by Barenblatt et al. (1960). Additionally, Warren and Root (1963) established an ideal system formed by matrix blocks separated by orthogonal fractures; they then obtained drawdown solutions considering the quasi-steady-state inter-porosity flow between the

matrixes and fractures in fractured aquifers. The transient inter-porosity flow models between the matrixes and fractures were presented by Kazemi (1969). We cannot judge which model is better or worse, but the quasi-steady-state model greatly simplifies several mathematical derivations (Önder, 1998). In recent decades, owing to its relative simplification and high efficiency, the double porosity model has been favoured by an increasing number of researchers (Moench, 1984; Hamm and Bidaux, 1996; Lods and Gouze, 2004; Mei et al., 2020). The head transient behaviour for pumping tests in fractured aquifers has been also discussed in compendiums of aquifer test analysis, e.g., Kruseman and de Ridder (1991), Batu (1998), Cheng (2000), and Walton (2006). A recent overview of flow models for well testing in fractured media was given by Nielsen (2007). At present, the continuous medium dual-porosity model has been widely used in the field of groundwater seepage and petroleum engineering (Boulton and Streitsova, 1977; Gerke and van Genuchten, 1993; Ge, 1997; Slimani and Tiab, 2008). However, owing to the complexity of underground geological conditions

* Corresponding author.

E-mail addresses: wanglei1986sp@foxmail.com (L. Wang), caijc@cug.edu.cn (J. Cai).

and fracture morphology, we still face new challenges. In the real world, fracture systems are not orthogonal. The distribution of fractures may be random, and the length, conductivity, and orientation of each fracture are different (Cai et al., 2017; Liu et al., 2018). To consider the fracture flow behaviour in a stricter sense, the flow in the fractures must be considered explicitly.

The discrete fracture networks (DFN) model can be used to accurately simulate the flow behaviour in fractures (Lee et al., 2001; Karimi et al., 2004). In the literature of groundwater and petroleum, scholars have attempted to use numerical methods to study the discrete fracture network (Olorode et al., 2013; Qiu et al., 2015; Xu et al., 2017). In most standard numerical methods, the whole domain is divided into small cells, and the drawdown and flow rate for each cell must be calculated in each timestep. To obtain an accurate drawdown distribution in each timestep, the area near the discrete fracture must be strictly encrypted. A 3D Voronoi mesh maker was presented by Olorode et al. (2013) to simulate flow behaviours for various complex fracture patterns. Xu et al. (2017) synthesized the embedded discrete fracture method into a numerical simulation. Although the numerical method can address the complex fracture problem with few assumptions, owing to the complexity of nonorthogonal grids and associated limitations of numerical computation, these approaches may increase the computational time needed for cases with a large number of cells and a small time step to obtain sufficiently accurate results. In addition, because of errors associated with numerical dispersion, early flow behaviours cannot be observed.

An alternative method is a semi-analytical method that is more flexible in calculation speed and does not need to be meshed in an entire aquifer (Wang et al., 2018a, 2018b). During recent decades, scholars have developed some models for fracture problems in the field of groundwater flow and petroleum engineering (Gringarten et al., 1974; Jenkins and Prentice, 1982; Sen, 1986; Cinco-Ley and Meng, 1988; Chen et al., 2016; Wang et al., 2018a, 2018b; Luo et al., 2019). As pioneers in the field, Gringarten et al. (1974) developed analytical solutions concerning groundwater flow towards fully penetrating vertical fractures. They presented a set of type curves for observation wells located at different positions around a finite length fracture. Jenkins and Prentice (1982) presented a linear (non-radial) flow model for an infinitesimally small aperture but an extensively long fracture. Sen (1986) provided a type curve for the linear to a pumping well, and the fracture storage capacity was also considered in his model. In the above three models, the authors assumed that the flow of a fluid in a fracture is infinitely conductive.

In this study, a semi-analytical model is developed to investigate the drawdown transient behaviour in discretely fractured aquifers with multiple finitely conductive fractures. First, the aquifer model and fracture model are established, and the analytical solutions in the aquifer system and fracture system are obtained using Laplace transform methodology. Then, a fracture network is discretized into fracture segments, and the flux and drawdown equivalent conditions in the Laplace space are applied in the fracture wall to couple the fluid flow in both systems. The final solutions for wellbore drawdown are presented and compared with the existing analytical solutions of a single fracture model (Cinco-Ley and Meng, 1988). In addition, the semi-analytical model is more general, which allows us to consider any mode of intersection or non-intersection among the fractures. Finally, an analysis of important flow characteristics and parameters influencing the factors of discrete fractures is also proposed. The main advantage of the solution in the Laplace domain is that it requires neither volumetric discretization nor the discretization of time, and it can be performed on demand.

2. Methodology

2.1. Basic assumption

In this study, we assumed that discrete fractures exist in confined

aquifers in two ways. The first is that discrete fractures do not intersect each other (Fig. 1a), whereas the second is that vertical intersections of some fractures occur (Fig. 1b). The detailed assumptions are as follows:

- (1) The confined aquifer is infinite, horizontal with a uniform thickness b , a hydraulic conductivity K_m , and an aquifer specific storage capacity S_{sm} , and the upper and lower boundaries of the confined aquifer are closed.
- (2) In the process of pumping, the temperature change in the aquifers is ignored.
- (3) Each well has a constant rate Q and can either intersect with the fracture or not.
- (4) A two-dimensional Darcy seepage occurs in the aquifers, and the radius of pumping well is r_w .
- (5) Because the width of the fracture is much smaller than its length, we assumed that a one-dimensional flow occurs in the fracture.
- (6) As shown in Fig. 2, the discrete fracture system contains N_f fractures with a full length L_{fn} , hydraulic conductivity K_{fn} , fracture width w_{fn} , angle θ_n with the x-axis, and the located position (x_{0fn}, y_{0fn}) , $n = 1, 2, \dots, N_f$.

2.2. The aquifer model

According to the above assumptions, the head governing equation in the aquifers can be described as:

$$\nabla K_m \nabla h_m + \sum_{e=1}^M \frac{Q_{we}}{b} \delta(x - x_{we}) \delta(y - y_{we}) + F_{f1}(t) = S_{sm} \frac{\partial h_m}{\partial t} \in \Omega \quad (1.1)$$

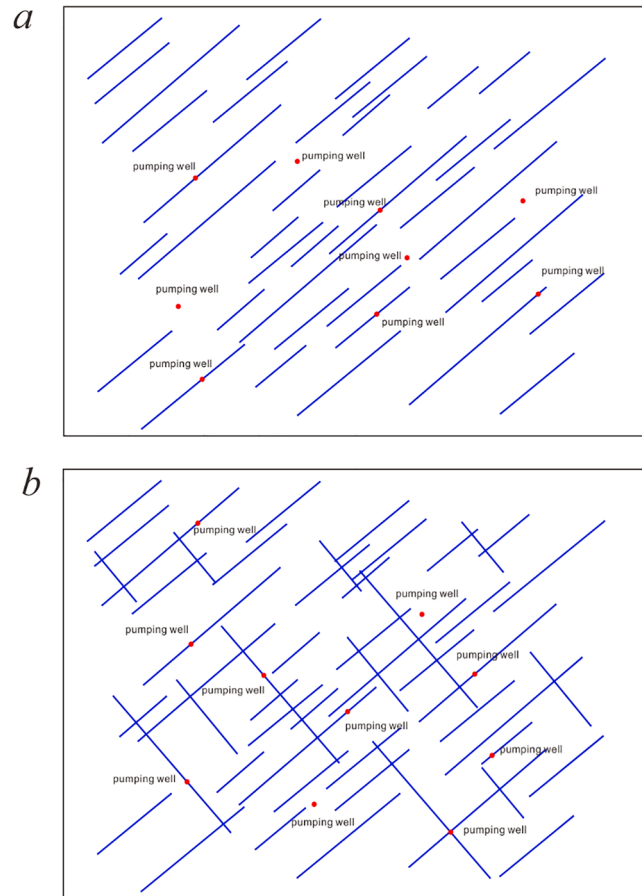


Fig. 1. Diagrammatic sketch for multiple pumping wells in a discretely fractured aquifer with multiple conductive fractures. (a) Non-intersection of discrete fractures and (b) intersection of partly discrete fractures.

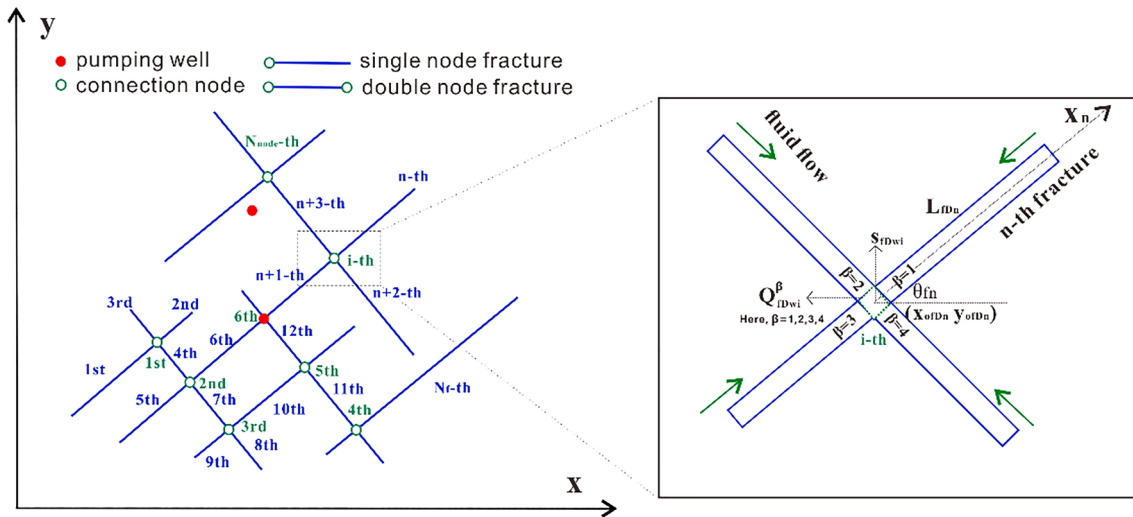


Fig. 2. Flow model for intersecting and conductive fractures in discretely fractured aquifers (the green number represents the node number, and the blue number represents the fracture number). (For interpretation of the references to colour in this figure legend, the reader is referred to the web version of this article.)

where:

$$F_{f1}(t) = \sum_{n=1}^{N_f} \int_0^{L_{fn}} \frac{1}{b} q_{fn,1}(u_n, t) \times \delta\left(x - x_{ofn} + \frac{w_{fn}}{2} \sin \theta_{fn} - u_n \cos \theta_{fn}\right) du_n + \sum_{n=1}^{N_f} \delta\left(y - y_{ofn} - \frac{w_{fn}}{2} \cos \theta_{fn} - u_n \sin \theta_{fn}\right) \times \int_0^{L_{fn}} \frac{1}{b} q_{fn,2}(u_n, t) \times \delta\left(x - x_{ofn} - \frac{w_{fn}}{2} \sin \theta_{fn} - u_n \cos \theta_{fn}\right) du_n \delta\left(y - y_{ofn} + \frac{w_{fn}}{2} \cos \theta_{fn} - u_n \sin \theta_{fn}\right) \quad (1.2)$$

where the operator $\nabla = (\partial/\partial x, \partial/\partial y)$, and δ is the Dirac delta function; h_m is hydraulic head in the aquifer (L), K_m is the hydraulic conductivity in the aquifer ($L T^{-1}$), S_m is the specific storage capacity in the aquifer (L^{-1}), t is the time (T), M is number of wells that does not intersect fractures, b is the aquifer thickness (L), (x_{we}, y_{we}) is the well location, (x, y) is the coordinate of any point, and Q_{we} is the pumping rate per unit of volume ($L^3 T^{-1}$). The superscript m represents the aquifer or matrix. L_{fn} is the n^{th} fracture length (L), $F_{f1}(t)$ is the fracture source sink term, u_n is the integral variable of the n^{th} fracture length (L), θ_{fn} is the angle between the n^{th} fracture and x-axis, (x_{ofn}, y_{ofn}) is the coordinate of the n^{th} fracture starting point (L), $q_{fn,1}$ is the first surface flow rate for the n^{th} fracture (L^2/T), $q_{fn,2}$ is the second surface flow rate for the n^{th} fracture (L^2/T), and u_n is location of the point source in the local fracture coordinate system for fracture n .

The aquifer is assumed to be initially at rest with a constant hydraulic head h_0 [L]. The well is pumped at a constant rate and, according to Eq. (1), an equation for aquifer drawdown can be written as follows:

$$\nabla T_m \nabla S_m + \sum_{\varepsilon=1}^M Q_{we} \delta(x - x_{we}) \delta(y - y_{we}) + F_f(t) = S_m \frac{\partial s_m}{\partial t} \quad \in \Omega \quad (2.1)$$

where:

$$F_f(t) = \sum_{n=1}^{N_f} \int_0^{L_{fn}} q_{fn,1}(u_n, t) \times \delta\left(x - x_{ofn} + \frac{w_{fn}}{2} \sin \theta_{fn} - u_n \cos \theta_{fn}\right) du_n + \sum_{n=1}^{N_f} \delta\left(y - y_{ofn} - \frac{w_{fn}}{2} \cos \theta_{fn} - u_n \sin \theta_{fn}\right) \times \int_0^{L_{fn}} q_{fn,2}(u_n, t) \times \delta\left(x - x_{ofn} - \frac{w_{fn}}{2} \sin \theta_{fn} - u_n \cos \theta_{fn}\right) du_n \delta\left(y - y_{ofn} + \frac{w_{fn}}{2} \cos \theta_{fn} - u_n \sin \theta_{fn}\right) \quad (2.2)$$

where $s_m = h_0 - h_m$ represents the drawdown in the aquifer (L), $S_m = S_{sm}b$ shows the overall aquifer storage coefficient of the aquifer, and $T_m = K_m b$ denotes the overall aquifer transmissivity ($L^2 T^{-1}$). For convenience, we used the dimensionless definition to make the above equation dimensionless, as follows: $S_{mD} = \frac{4\pi T_m S_m}{Q_r} x_D = \frac{x}{L_r}$, $y_D = \frac{y}{L_r}$, $x_{wDe} = \frac{x_{we}}{L_r}$, $y_{wDe} = \frac{y_{we}}{L_r}$, $L_{fDn} = \frac{L_{fn}}{L_r}$, $t_D = \frac{T_m t}{S_m L_r^2}$, $Q_{wDe} = \frac{Q_{we}}{Q_r}$, $q_{fDn,1} = \frac{q_{fn,1} L_r}{Q_r}$, $q_{fDn,2} = \frac{q_{fn,2} L_r}{Q_r}$, where (x_{we}, y_{we}) is the ε^{th} well location in the aquifer (L), Q_r is the reference flow rate ($L^3 T^{-1}$), and L_r is the reference length (L). Through the dimensionless definitions, Eq. (2) is transformed as follows:

$$\nabla^2 s_{mD} + F_{WD}(t_D) + F_{fD}(t_D) = \frac{\partial s_{mD}}{\partial t_D} \quad \in \Omega_D \quad (3.1)$$

and:

$$F_{WD} = \sum_{\varepsilon=1}^M 4\pi Q_{wDe} \delta(x_D - x_{wDe}) \delta(y_D - y_{wDe}) \quad (3.2)$$

$$F_{fD}(t_D) = \sum_{n=1}^{N_f} \int_0^{L_{fDn}} 4\pi q_{fDn,1}(u_{Dn}, t_D) \times \delta\left(x_D - x_{ofDn} + \frac{w_{fDn}}{2} \sin \theta_{fn} - u_{Dn} \cos \theta_{fn}\right) du_{Dn} + \sum_{n=1}^{N_f} \int_0^{L_{fDn}} 4\pi q_{fDn,2}(u_{Dn}, t_D) \times \delta\left(x_D - x_{ofDn} - \frac{w_{fDn}}{2} \sin \theta_{fn} - u_{Dn} \cos \theta_{fn}\right) du_{Dn} \times \delta\left(y_D - y_{ofDn} - \frac{w_{fDn}}{2} \cos \theta_{fn} - u_{Dn} \sin \theta_{fn}\right) \quad (3.3)$$

where s_{mD} is the dimensionless drawdown for the aquifers, (x_{wDe}, y_{wDe}) is the dimensionless well coordinate of the ε^{th} well, $F_{fD}(t_D)$ is the dimensionless fracture source sink term, $F_{WD}(t_D)$ is the dimensionless well source sink term, (x_{wDe}, y_{wDe}) is the ε^{th} dimensionless well location in the aquifer, (x_D, y_D) is the dimensionless coordinate of any point, (x_{ofDn}, y_{ofDn}) is the dimensionless coordinate of the n^{th} fracture starting point, u_{Dn} is the dimensionless integral variable of the n^{th} fracture length (L),

$$\begin{aligned} \tilde{s}_{mD}(x_D, y_D, p) = & \sum_{\varepsilon=1}^M \tilde{Q}_{wDe}(p) \xi_{\varepsilon}(x_D, y_D, x_{wDe}, y_{wDe}) + \sum_{n=1}^{N_f} \int_0^{L_{fDn}} \tilde{q}_{fDn,1}(u_{Dn}, p) \psi_{n,1}(x_D, y_D, x_{ofDn}, y_{ofDn}, \theta_{fDn}, p, u_{Dn}) du_{Dn} + \\ & \sum_{n=1}^{N_f} \int_0^{L_{fDn}} \tilde{q}_{fDn,2}(u_{Dn}, p) \psi_{n,2}(x_D, y_D, x_{ofDn}, y_{ofDn}, \theta_{fDn}, p, u_{Dn}) du_{Dn} \end{aligned} \quad (6.1)$$

L_{fDn} is the n^{th} fracture dimensionless length, $q_{fDn,1}$ is the first surface dimensionless flow rate for the n^{th} fracture, $q_{fDn,2}$ is the second surface dimensionless flow rate for the n^{th} fracture, Q_{wDe} is the dimensionless well flow rate of the ε^{th} well, t_D is dimensionless time, L_{fDn} is the dimensionless fracture length, and n is the subscript representing the n^{th} fracture. The drawdown of the aquifer before pumping would be zero, and the initial condition can be given as follows:

$$s_{mD}(x_D, y_D, 0) = 0 \quad (4)$$

The boundary condition at infinity is given as follows

$$s_{mD}(\infty, \infty, t_D) = 0 \quad (5)$$

Combining Eqs. (3)–(5), using the Laplace transform and Fourier transform (see S1 of supplementary document), the dimensionless drawdown solution for the aquifer can be obtained as follows:

where:

$$\xi_n = 2 \times K_0 \left(\sqrt{p} \sqrt{(x_D - x_{wDe})^2 + (y_D - y_{wDe})^2} \right) \quad (6.2)$$

and:

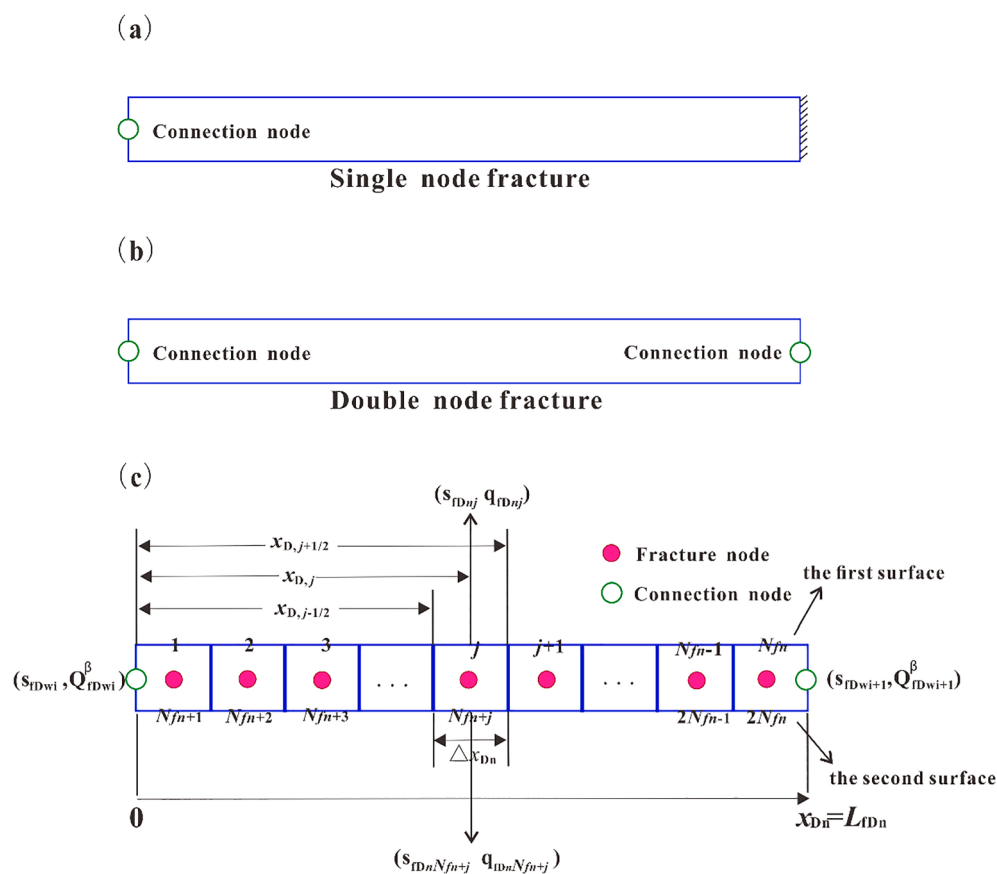


Fig. 3. Diagrammatic sketch of one-dimensional fracture flow in the discrete fracture for (a) a single node model, (b) a double node model, and (c) a discretization of a double node fracture for two surfaces.

$$\psi_{n,1} = 2 \times K_0 \left[\sqrt{p} \sqrt{\left(x_D - x_{ofDn} + \frac{w_{fDn}}{2} \sin \theta_{fn} - u_{Dn} \cos \theta_{fn} \right)^2 + \left(y_D - y_{ofDn} - \frac{w_{fn}}{2} \cos \theta_{fn} - u_{Dn} \sin \theta_{fn} \right)^2} \right] \quad (6.3)$$

$$\psi_{n,2} = 2 \times K_0 \left[\sqrt{p} \sqrt{\left(x_D - x_{ofDn} - \frac{w_{fDn}}{2} \sin \theta_{fn} - u_{Dn} \cos \theta_{fn} \right)^2 + \left(y_D - y_{ofDn} + \frac{w_{fn}}{2} \cos \theta_{fn} - u_{Dn} \sin \theta_{fn} \right)^2} \right] \quad (6.4)$$

As shown in Fig. 3c, the two surfaces of the n^{th} fracture is divided into $2N_{fn}$ segments, and thus the j -th segment drawdown on the surface can be obtained from Eq. (6) as:

$$\begin{aligned} \tilde{s}_{mD,nj}(p) = & \sum_{e=1}^M \tilde{Q}_{wDe}(p) \xi_n(x_{Dnj}, y_{Dnj}, x_{wDe}, y_{wDe}) + \sum_{n=1}^{N_f} \sum_{i=1}^{N_{fn}} \int_{(i-1)\Delta x_{Dn}}^{i\Delta x_{Dn}} \tilde{q}_{fDni,1}(u_{Dn}, p) \psi_n(x_{Dnj}, y_{Dnj}, x_{ofDni}, y_{ofDni}, \theta_{fni}, p, u_{Dn}) du_{Dn} \\ & + \sum_{n=1}^{N_f} \sum_{i=1}^{N_{fn}} \int_{(i-1)\Delta x_{Dn}}^{i\Delta x_{Dn}} \tilde{q}_{fDni,2}(u_{Dn}, p) \psi_n(x_{Dnj}, y_{Dnj}, x_{ofDni}, y_{ofDni}, \theta_{fni}, p, u_{Dn}) du_{Dn} \end{aligned} \quad (7.1)$$

If we want to calculate drawdown for any location, Eq. (7-1) can be replaced by

$$\begin{aligned} \tilde{s}_{mD}(p, x_D, y_D) = & \sum_{e=1}^M \tilde{Q}_{wDe}(p) \xi_n(x_D, y_D, x_{wDe}, y_{wDe}) + \sum_{n=1}^{N_f} \sum_{i=1}^{N_{fn}} \int_{(i-1)\Delta x_{Dn}}^{i\Delta x_{Dn}} \tilde{q}_{fDni,1}(u_{Dn}, p) \psi_n(x_D, y_D, x_{ofDni}, y_{ofDni}, \theta_{fni}, p, u_{Dn}) du_{Dn} \\ & + \sum_{n=1}^{N_f} \sum_{i=1}^{N_{fn}} \int_{(i-1)\Delta x_{Dn}}^{i\Delta x_{Dn}} \tilde{q}_{fDni,2}(u_{Dn}, p) \psi_n(x_D, y_D, x_{ofDni}, y_{ofDni}, \theta_{fni}, p, u_{Dn}) du_{Dn} \end{aligned} \quad (7.2)$$

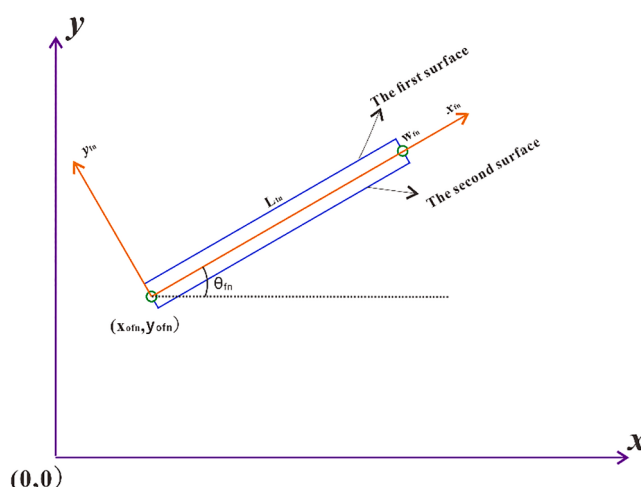


Fig. 4. The translation and rotation transformation of Cartesian coordinates.

where $\tilde{s}_{mD,nj}$ is the draw Cinco down in the Laplace space for the j^{th} segment of the n^{th} fracture, \tilde{Q}_{wDe} is the well flow rate in Laplace space for the e^{th} well, $\tilde{q}_{fDni,1}$ is the dimensionless flow rate of the first surface in the

Laplace space for the i^{th} segment of the n^{th} fracture, $\tilde{q}_{fDni,2}$ is the dimensionless flow rate of the second surface in the Laplace space for the i^{th} segment of the n^{th} fracture, (x_{Dnj}, y_{Dnj}) is the dimensionless middle point coordinate for the j^{th} segment of the n^{th} fracture, (x_{ofDni}, y_{ofDni}) is

the dimensionless starting point coordinate for the i^{th} segment of the n^{th} fracture, (x_{wDe}, y_{wDe}) is the dimensionless e^{th} well location in the aquifer, p is the Laplace transformed time parameter, Δx_{Dn} is the dimensionless segment length of the n^{th} fracture, θ_{fni} is the angle between the i^{th} segment of the n^{th} fracture and the x -axis, N_f is the total fracture number, and N_{fn} is the fracture segment number per fracture surface for the n^{th} fracture.

2.3. Discrete fracture model

Discrete fracture systems in aquifers are composed of two kinds of simple fractures. One comprises a node at one end with the other end being closed, which is called a single node model (Fig. 3a). Another case is that both ends are nodes, which is called a double node model (Fig. 3b). The single node model is a special case of double node model, so to generalize our proposed model, we describe here the derivation of the double node model. As shown in Fig. 3c, the drawdown and flow rate for double nodes are considered to be unknowns.

Because the fracture volume is exceedingly small compared with the

volume of the entire aquifer, the response is assumed to instantaneously respond to external changes, reaching a pseudo-steady state in the fracture. Although the response of unsteady-state models is different from that of the PSS model, the difference becomes exceedingly small and almost disappears within a short time period. Alternatively, the overall aquifer storage coefficient of the fracture is so small that the effect of storage coefficient can be neglected (Zeng, 2008). As a result, the drawdown equation can be given as:

$$\frac{\partial}{\partial x_{fn}} \left[K_{fn} \frac{\partial s_{fn}}{\partial x_{fn}} \right] + \frac{\partial}{\partial y_{fn}} \left[K_{fn} \frac{\partial s_{fn}}{\partial y_{fn}} \right] = 0, \quad \begin{cases} 0 < x_{fn} < L_{fn} \\ -\frac{w_n}{2} < y_{fn} < \frac{w_n}{2} \end{cases} \quad (8)$$

According to Darcy's law, the terms of $K_{fn} \frac{\partial s_{fn}}{\partial x_{fn}}$ and $K_{fn} \frac{\partial s_{fn}}{\partial y_{fn}}$ represent the flow velocity parallel to the fracture-length and fracture-width directions, respectively. Note that the local spatial coordinates in the n^{th} fracture are denoted as (x_{fn}, y_{fn}) , and the global spatial coordinates in the aquifer are denoted as (x, y) . After translation and rotation transformation (Fig. 4), the relationship between local coordinates and global coordinates is as follows

$$x_{fn} = (x - x_{ofn}) \cos(\theta_{fn}) + (y - y_{ofn}) \sin(\theta_{fn}) \quad (9)$$

$$y_{fn} = (y - y_{ofn}) \cos(\theta_{fn}) - (x - x_{ofn}) \sin(\theta_{fn}) \quad (10)$$

The relationship equations imply functional relationship between local coordinates and global coordinates. If the local coordinate position is given, the corresponding global coordinate can be calculated.

From the perspective of the entire confined aquifer, the fracture width is exceedingly small compared with the fracture length. On the two interface surfaces of fracture, the flow rate will be equal to the aquifer

$$\begin{aligned} K_{fn} \frac{\partial s_{fn}}{\partial y_{fn}} \Big|_{y_{fn}=\frac{w_{fn}}{2}} &= K_m \frac{\partial s_m}{\partial l} \Big|_{l=f_{1n}(x,y)} \quad 0 < x_{fn} < L_{fn}, y_{fn} = w_{fn}/2 \\ K_{fn} \frac{\partial s_{fn}}{\partial y_{fn}} \Big|_{y_{fn}=-\frac{w_{fn}}{2}} &= K_m \frac{\partial s_m}{\partial l} \Big|_{l=f_{2n}(x,y)} \quad 0 < x_{fn} < L_{fn}, y_{fn} = -w_{fn}/2 \end{aligned} \quad (11)$$

where, as shown in Fig. 4, $y_{fn} = w_{fn}/2$ and $y_{fn} = -w_{fn}/2$ represent the first surface and the second surface of the n^{th} fracture in local coordinate system, and $l = f_{1n}(x,y)$ and $l = f_{2n}(x,y)$ represents the first surface and the second surface of the n^{th} fracture in global coordinate system. According to functional relationship between local coordinates and global coordinates shown in Eqs. (9) and (10), global coordinate (x, y) can be calculated when the local coordinate (x_{fn}, y_{fn}) is given. The value range of x_{fn} and y_{fn} can be found in Eq. (11)

Taking the integral average of the drawdown across the fracture width (in the y direction, Eq. (8) is similarly to Strack (1989):

$$\frac{\partial}{\partial x_{fn}} \left[K_{fn} \frac{\partial s_{fn}}{\partial x_{fn}} \right] + \left[K_{fn} \frac{\partial s_{fn}}{\partial y_{fn}} \Big|_{y_{fn}=\frac{w_{fn}}{2}} - K_{fn} \frac{\partial s_{fn}}{\partial y_{fn}} \Big|_{y_{fn}=-\frac{w_{fn}}{2}} \right] = 0 \quad (12)$$

Substituting flux equivalent conditions Eq. (11) into (12), Eq. (12) will be replaced by

$$\frac{\partial}{\partial x_{fn}} \left[K_{fn} \frac{\partial s_{fn}}{\partial x_{fn}} \right] + \left[K_m \frac{\partial s_m}{\partial l} \Big|_{l=f_{1n}(x,y)} - K_m \frac{\partial s_m}{\partial l} \Big|_{l=f_{2n}(x,y)} \right] = 0 \quad (13)$$

On the first surface of the fracture, the flux condition can be given as follows:

$$bL_{fn} K_m \frac{\partial s_m}{\partial l} \Big|_{l=f_{1n}(x,y)} = -q_{fn,1} L_{fn} \quad (14)$$

On the second surface of the fracture, the flux condition can be given as follows:

$$bL_{fn} K_m \frac{\partial s_m}{\partial l} \Big|_{l=f_{2n}(x,y)} = -q_{fn,2} L_{fn} \quad (15)$$

According to Darcy's law, the cross-sectional flow rate on the left node of the fracture can be given as follows:

$$-w_n b K_{fn} \frac{\partial s_{fn}}{\partial x_{fn}} \Big|_{x_{fn}=0} = Q_{fwi} \quad (16)$$

The flow rate condition on the right node of the fracture is as follows:

$$-w_n b K_{fn} \frac{\partial s_{fn}}{\partial x_{fn}} \Big|_{x=L_{fn}} = Q_{fw(i+1)} \quad (17)$$

where K_{fn} is the hydraulic conductivity in the n^{th} fracture (LT^{-1}), w_n is the n^{th} fracture width (L), s_{fn} is the drawdown in the n^{th} fracture (L), and Q_{fwi} is the i^{th} node flow rate in the n^{th} fracture (L^3T^{-1}).

The absolute values of Q_{fwi} and $Q_{fw(i+1)}$ represent the magnitude of the flow rate, and the signs represent the type of sink or source. A negative indicates the injection/source, and a positive indicates the extraction/sink. The type of sink or source is automatically determined by the mass balance principle on the interconnection among different fracture units.

Eqs. (13)–(17) form the discrete fracture drawdown equations. We can use the following dimensionless definitions to make the above equation dimensionless as follows:

$C_{fDn} = \frac{K_{fn} w_n}{K_m L_r}$, $s_{fDn} = \frac{4\pi T_m s_{fn}}{Q_r}$, $Q_{fDwi} = \frac{Q_{fwi}}{Q_r}$, $Q_{fDw(i+1)} = \frac{Q_{fw(i+1)}}{Q_r}$, $l_D = \frac{l}{L_r}$ where C_{fDn} is the dimensionless n^{th} fracture conductivity, s_{fDn} is the dimensionless drawdown in the n^{th} fracture, and Q_{fDwi} is the i^{th} node dimensionless flow rate in the n^{th} fracture. Through the dimensionless definitions, Eq. (13) can be transformed as follows:

$$\frac{\partial^2 s_{fDn}}{\partial x_{fDn}^2} + \left[\frac{1}{C_{fDn}} \frac{\partial s_{mD}}{\partial l_D} \Big|_{l_D=f_{1n}(x_D,y_D)} - \frac{1}{C_{fDn}} \frac{\partial s_{mD}}{\partial l_D} \Big|_{l_D=f_{2n}(x_D,y_D)} \right] = 0 \quad (18)$$

Eq. (14) becomes

$$\frac{\partial s_{mD}}{\partial l_D} \Big|_{l_D=f_{1n}(x_D,y_D)} = -4\pi q_{fDn,1} \quad (19)$$

Eq. (15) becomes

$$\frac{\partial s_{mD}}{\partial l_D} \Big|_{l_D=f_{2n}(x_D,y_D)} = -4\pi q_{fDn,2} \quad (20)$$

Eq. (16) becomes:

$$\frac{\partial s_{fDn}}{\partial x_{fDn}} \Big|_{x_{fDn}=0} = -Q_{fDwi} \frac{4\pi}{C_{fDn}} \quad (21)$$

Eq. (17) becomes:

$$\frac{\partial s_{fDn}}{\partial x_{fDn}} \Big|_{x_{fDn}=L_{fn}} = -Q_{fDw(i+1)} \frac{4\pi}{C_{fDn}} \quad (22)$$

Eqs. (18)–(22) constitute a system of dimensionless drawdown equations of discrete fractures. By using the double integral method (See S2 of supplementary document), we can obtain its Laplace-transform solution as follows:

$$\tilde{s}_{fDwi} - \tilde{s}_{fDn}(x_{fDn}) = \frac{4\pi}{C_{fDn}} x_{fDn} \tilde{Q}_{fDwi} - \frac{4\pi}{C_{fDn}} \int_0^{x_{fDn}} \int_0^v \tilde{q}_{fDn,1}(u) du dv + \frac{4\pi}{C_{fDn}} \int_0^{x_{fDn}} \int_0^v \tilde{q}_{fDn,2}(u) du dv \quad (23)$$

where \tilde{s}_{fDwi} is the drawdown in Laplace space for the i^{th} node, \tilde{s}_{fDn} is the drawdown at x_{fDn} in the Laplace space, \tilde{Q}_{fDwi} is the flow rate in the Laplace space for the i^{th} node, $\tilde{q}_{fDn,1}$ is the flow rate of the first surface in the Laplace space, $\tilde{q}_{fDn,2}$ is the flow rate of the second surface in the Laplace space, and C_{fDn} is the dimensionless fracture conductivity for the n^{th} fracture. As shown in Fig. 3c, we then discretize the above equation, and if the fracture surface is divided into $2N_{fn}$ segments, for j^{th} segment of the n^{th} fracture (see Fig. 3c), Eq. (23) would have the following transformation:

$$\begin{aligned} \tilde{s}_{fDnj}(x_{fDnj}) = & \tilde{s}_{fDwi}(p) - \frac{4\pi}{C_{fDn}} x_{fDnj} \tilde{Q}_{fDwi} + \frac{4\pi}{C_{fDn}} \left\{ \sum_{\varepsilon=1}^{j-1} \tilde{q}_{fDne,\varepsilon,1}(p) \left[\frac{\Delta x_{fDn}^2}{2} + \Delta x_{fDn}(x_{fDnj} - \varepsilon \Delta x_{fDn}) \right] + \frac{\Delta x_{fDn}^2}{8} \tilde{q}_{fDnj,1}(s) \right\} - \frac{4\pi}{C_{fDn}} \left\{ \sum_{\varepsilon=1}^{j-1} \tilde{q}_{fDne,\varepsilon,2}(p) \left[\frac{\Delta x_{fDn}^2}{2} + \Delta x_{fDn}(x_{fDnj} - \varepsilon \Delta x_{fDn}) \right] \right. \\ & \left. + \frac{\Delta x_{fDn}^2}{8} \tilde{q}_{fDnj,2}(s) \right\} \end{aligned} \quad (24)$$

where x_{fDnj} is the middle point for the j^{th} segment of the n^{th} fracture, \tilde{s}_{fDnj} is the dimensionless drawdown in the Laplace space for the j^{th} segment of the n^{th} fracture, \tilde{s}_{fDwi} is the dimensionless drawdown for i^{th} node in the Laplace space for the j^{th} segment of the n^{th} fracture, Δx_{fDn} is the dimensionless segment length of the n^{th} fracture. The rest of the symbols are already defined above.

2.4. Semi-analytical solution of the coupled model

To obtain the final semi analytical solution, we must couple the

aquifer model with the discrete fracture model. Here, let us consider the unknowns. N_f is the number of fractures, and each fracture has N_{fn} segments. Thus, the total number of fracture surface fluxes is:

$$N_{tsur} = \sum_{n=1}^{N_f} 2 \times N_{fn} \quad (25)$$

In addition, N_{node} is the number of nodes in the fracture. Suppose that the i^{th} node has n_i branches, as shown in Fig. 2, each node has n_i unknown flow rate Q_{fDwi}^β (for example, if the i^{th} node is linked to the four fractures, then n_i is equal to 4 and $\beta = 1, 2, 3, 4$, as shown in Fig. 2);

thus, the number of the total unknown flow rate is

$$N_{trat} = \sum_{i=1}^{N_{node}} n_i \quad (26)$$

Each node has one unknown drawdown s_{fDwi} ; thus, the total number of the unknown drawdown is N_{node} . Therefore, the total number of unknowns is $N_{tsur} + N_{trat} + N_{node}$. The unknowns in Laplace space can be provided in a vector form:

$$\vec{X} = \left[\underbrace{\tilde{q}_{fD11,1}, \tilde{q}_{fD12,1}, \dots, \tilde{q}_{fD1N_{f1},1}, \dots, \tilde{q}_{fDn1,1}, \tilde{q}_{fDn2,1}, \dots, \tilde{q}_{fDnN_{fn},1}, \tilde{q}_{fD11,2}, \tilde{q}_{fD12,2}, \dots, \tilde{q}_{fD1N_{f1},2}, \dots, \tilde{q}_{fDn1,2}, \tilde{q}_{fDn2,2}, \dots, \tilde{q}_{fDnN_{fn},2}, \tilde{Q}_{fDw1}^1, \tilde{Q}_{fDw1}^2, \dots, \tilde{Q}_{fDw1}^{n_1}, \dots, \tilde{Q}_{fDwN_{node}}^1, \dots, \tilde{Q}_{fDwN_{node}}^{n_{node}}}_{T} \right. \\ \left. , \tilde{Q}_{fDwN_{node}}^2, \dots, \tilde{Q}_{fDwN_{node}}^{n_{node}}, \underbrace{\tilde{s}_{fDw1}, \tilde{s}_{fDw2}, \dots, \tilde{s}_{fDwN_{node}}}_{N_{node}} \right] \quad (27)$$

$$\tilde{Q}_{fDwi}^{\beta} = \sum_{\varepsilon=1}^{N_{fn}} \tilde{q}_{fDne,1} \cdot \frac{L_{fDn}}{N_{fn}} + \sum_{\varepsilon=1}^{N_{fn}} \tilde{q}_{fDne,2} \cdot \frac{L_{fDn}}{N_{fn}} \quad i = 1, 2, \dots, N_{node} \quad \beta = 1, 2, \dots, n_i \quad (30)$$

According to the continuity condition that the aquifer drawdown s_{Dn} in Eq. (7) is continuous to the fracture drawdown s_{fD} in Eq. (24) on the surface of the fracture, the following equation can be given:

$$\tilde{s}_{mD,ij}(p) = \tilde{s}_{fDnij}(x_{Dj}) \quad n = 1, 2, \dots, N_f \quad j = 1, 2, \dots, N_{fn}, N_{fn} + 1, \dots, 2N_{fn} \quad (28)$$

$$\tilde{Q}_{fDwi}^{\beta} + \tilde{Q}_{fDw(i+1)}^{\beta} = \sum_{\varepsilon=1}^{N_{fn}} \left(\tilde{q}_{fDne,1} + \tilde{q}_{fDne,2} \right) \cdot \frac{L_{fDn}}{N_{fn}} \quad i = 1, 2, \dots, N_{node} \quad \beta = 1, 2, \dots, n_i \quad (31)$$

There are N_{tsur} equations in Eq. (28). If there is no well outflow at the node, the total flow of the node is equal to zero. Alternately, if there is a well at a certain node, the sum of the total flow rate should be equal to the well flow rate. Thus, the following equation can be given:

$$\sum_{\beta=1}^{n_i} \tilde{Q}_{fDwi}^{\beta} = \begin{cases} 0 & \text{for no well rate} \\ \tilde{Q}_{fDwi}^{\text{well}} & \text{for well rate} \end{cases}$$

There are N_{node} equations in Eq. (29). Chen et al. (2016) proposed a method to address the problem of intersection flow by manually judging

$$\tilde{s}_{fDwi} - \tilde{s}_{fDw(i+1)} = \frac{4\pi}{C_{fDn}} L_{fDn} \tilde{Q}_{fDwi} - \frac{4\pi}{C_{fDn}} \sum_{\varepsilon=1}^{N_{fn}} \left[\tilde{q}_{fDne,1}(p) + \tilde{q}_{fDne,2}(p) \right] \times [\Delta x_n^2 + \Delta x_n (L_{fDn} - \varepsilon \Delta x_n)] \quad (32)$$

the flow direction. However, their method was extraordinarily complex and difficult to implement in large-scale fracture crossing. To obtain an accurate simulation of fracture intersections, we used the principle of mass balance to enable the flow redirection automatically rather than artificially as in Chen et al. (2016); this was ensured by restricting the magnitude of the source on interconnections from different fracture panels. This can solve the problem of intersection flow calculations of multiple fractures. The model in Eq. (29) makes it unnecessary for us to judge the flow direction of an intersection. As shown in Fig. 2, the i -th node is linked into n_i fractures and it will produce n_i total flow rate for this node. For example, there are four fractures linked to the i -th node, therefore, there would be four flow rate in this node. In other words, each fracture connected to this node has a total flow, the relationship between each flow rate and the flux of the fracture segment can be given as follows:

There are N_{trat} equations in Eq. (30). Notice that there are $N_{tsur} + N_{trat} + N_{node}$ unknowns, and there are $N_{tsur} + N_{trat} + N_{node}$ equations. Equation (30) is suitable for single node model (see Fig. 2). However, for double node model (see Fig. 3c), the sum of the flux on the two fracture surface should be equal to the sum of the total flow rate of the two nodes. The relationship in Eq. (30) will be replaced by:

The above equation shows that whether the i^{th} node is or the $(i+1)^{\text{th}}$ node is used as a reference point, only one equation can be created. However, before that, each node will list a different equation such as Eq. (30). In other words, for each double node fracture, the number of

$$i = 1, 2, \dots, N_{node} \quad (29)$$

equations is reduced by one, so we must add an auxiliary drawdown equation for each additional double node fracture, which is given by:

Eqs. (25)–(32) constitute a linear equation system of the Laplace space, which can be solved by the Gaussian elimination method. Then, the derived solution is brought into equation (7–1), and we can obtain any wellbore drawdown of the Laplace space. Substituting fracture surface flow rate and nodal flow rate into Eq. (7–2), the drawdown in any location (x_D, y_D) can be calculated. The final wellbore drawdown in the real time domain can be obtained by the Stehfest (1970) numerical inversion (see S3 of supplementary document). Kuhlman and Neuman (2009), Kuhlman and Kristopher (2013) has evaluated the Laplace-Space numerical approaches in detail. The well radius for the final wellbore drawdown solution is given by

$$r_{wD} = \sqrt{(x_D - x_{wD})^2 + (y_D - y_{wD})^2} \quad (33)$$

where r_{wD} is the dimensionless wellbore radius, which is set to 0.001 in this study.

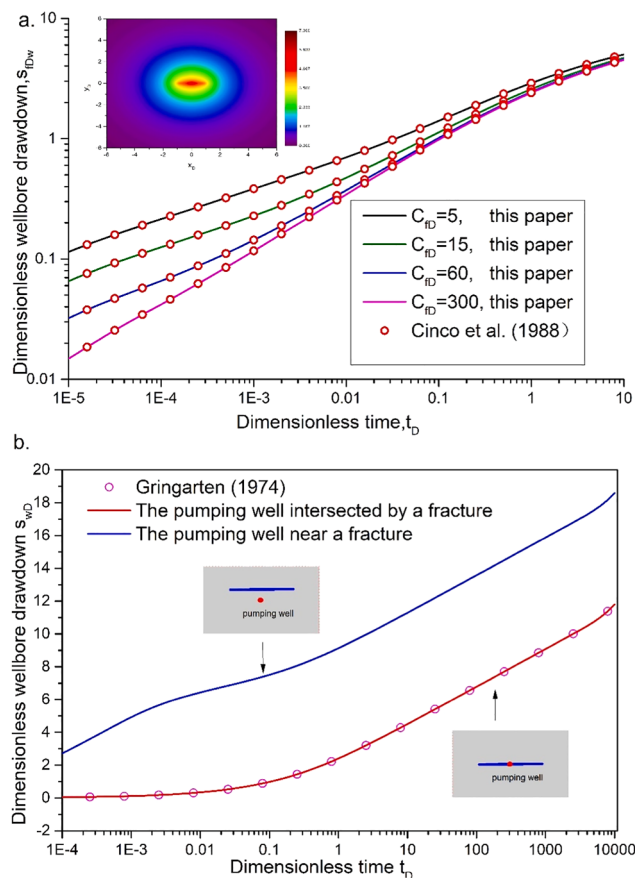


Fig. 5. Proposed drawdown solution compared with the literature (Cinco-Ley and Meng, 1988; Gringarten et al., 1974). (a) The presented drawdown solutions compared with Cinco-Ley and Meng (1988) under different conductivity ($C_{fD} = 5, 15, 60, 300$) for a pumping well intersected by a finite conductive fracture and (b) The presented drawdown solutions compared with Gringarten et al. (1974) for an infinite conductive fracture (red line represents the drawdown solution for a pumping well intersected by one fracture and blue line represents drawdown solutions for a pumping well near a fracture). (For interpretation of the references to colour in this figure legend, the reader is referred to the web version of this article.)

3. Results and discussion

In this section, we will discuss cases for a pumping well in discretely fractured aquifers with multiple finitely conductive fractures. In the fractured aquifers, any fracture can be described by parameters such as length, aperture, and orientation (Sen, 1986; Xu et al., 2017; Wang et al., 2018a, 2018b), which is different from the double-porosity model. Fractures can be divided into isolated and interconnected network fracture types. Of course, a pumping well can be arbitrarily arranged in a fracture or matrix. We will thus discuss how the drawdown behaviour of a pumping well can change. In this analysis, we used the drawdown derivative curve analysis method (Bourdet et al., 1983).

3.1. Comparison with the literature for a well intersected by a conductive fracture

Prior to this article, Cinco-Ley and Meng (1988) proposed that a well can be crossed by a finitely conductive fracture, which was named as an extended well (Sen, 1986). Fig. 5a shows presented drawdown solutions compared with Cinco-Ley and Meng (1988) under different conductivity for a pumping well intersected by a finite conductive fracture. Thus, for convenience, we simulated this simple case. In our model, the fracture length L_{fD} was set to 2, and the fracture conductivity C_{fD} was set to 5, 15,

60, and 300, respectively. The pumping well was located at ($x_D = 0, y_D = 0$). The fracture centre was located at ($x_D = 0, y_D = 0$), and the angle with the axis was 0° . The solution (Cinco-Ley and Meng, 1988) is the dimensionless pressure solution and it can be found that the proposed solution is in good agreement with their solution. In the field of well test analyses for hydrology and petroleum, the dimensionless drawdown equation is similar to the dimensionless pressure equation in the literature, so their results are comparable. However, the previous solution (Cinco-Ley and Meng, 1988) is only a special case of the proposed model. The subgraph in Fig. 5a shows the drawdown distribution of the dimensionless time. The shape of equipotential lines near the extended wells is elliptical, which implies that an elliptical flow will occur for an extended well in a confined aquifer. Fig. 5b shows drawdown solutions compared with Gringarten et al. (1974) for an infinite conductive fracture (red line represents the drawdown solution for a pumping well intersected by one fracture and blue line represents drawdown solutions for a pumping well near a fracture). We compared our solution with their solution (Gringarten et al., 1974) in this specific case. The fracture length L_{fD} was set to 2, and the distance between the fracture and the pumping well was set to 0.02. Fig. 5b shows that the drawdown curves can completely coincide. However, their results are exceedingly limited. First, their method can only calculate a finite length fracture, and fractures are infinitely conductive. Second, they only assumed that the well and the fracture intersected; if a well and fracture were to separate, their method could not calculate the drawdown. In this study, from comparing a simple case, we found that the drawdown was exceedingly different depending on whether the well and fracture intersected or not. The proposed model in this study allows us to consider the problems of pumping tests in many complex fracture networks, including parallel uncrossed fracture networks, arbitrary distribution non-intersected fracture networks, intersected fracture networks with some isolated fractures.

3.2. Drawdown behaviour for a pumping well near a conductive natural fracture

Fig. 6 shows the drawdown behaviour for a pumping well near a conductive natural fracture under the effect of different fracture parameters. The analysis of such an example is helpful for us to understand the drawdown behaviour in a more complex fracture system. The derivative of the drawdown can better reflect the flow characteristics of confined aquifers (Warren and Root, 1963; Moench, 1984; Hamm and Bidaux, 1996). As shown in Fig. 6, the derivative of the drawdown for all sub-figures shows three flow periods: an early time radial flow period, transient flow period, and late time quasi-radial flow period. Whether in the early or late stage of flow, the derivative of the drawdown shows one constant straight, and one dip valley appears in the transient flow period.

Fig. 6a shows the effect of dimensionless distance D between the fracture and pumping well for the drawdown and its derivative. The dimensionless distance D was set to 0.03, 0.05 and 0.1, respectively. In this case, the dimensionless fracture length L_{fD} was set to 2. The semi-log plot wellbore drawdown vs. time in the early time radial flow period yielded a straight line whose slope was related to the hydraulic conductivity of the confined aquifer. The end time of early time radial flow was related to the distance D and the shorter the distance was, the earlier the end time was. Next, the drawdown curves with a shorter distance caused a smaller drawdown loss; as this was useful for pumping, implying that pumping wells should be drilled near natural fractures. The log-log plot wellbore drawdown derivative vs. time in the transient flow period yielded one whose depth was related to the distance. A shorter distance would cause a deeper dip valley and an earlier starting time. Fig. 6b shows the effect of dimensionless natural fracture length L_{fD} on drawdown and its derivative. The dimensionless distance L_{fD} was set to 0.5, 2 and 4, respectively. The distance between a pumping well and a natural fracture D was set to 0.05. The semi-log plot wellbore

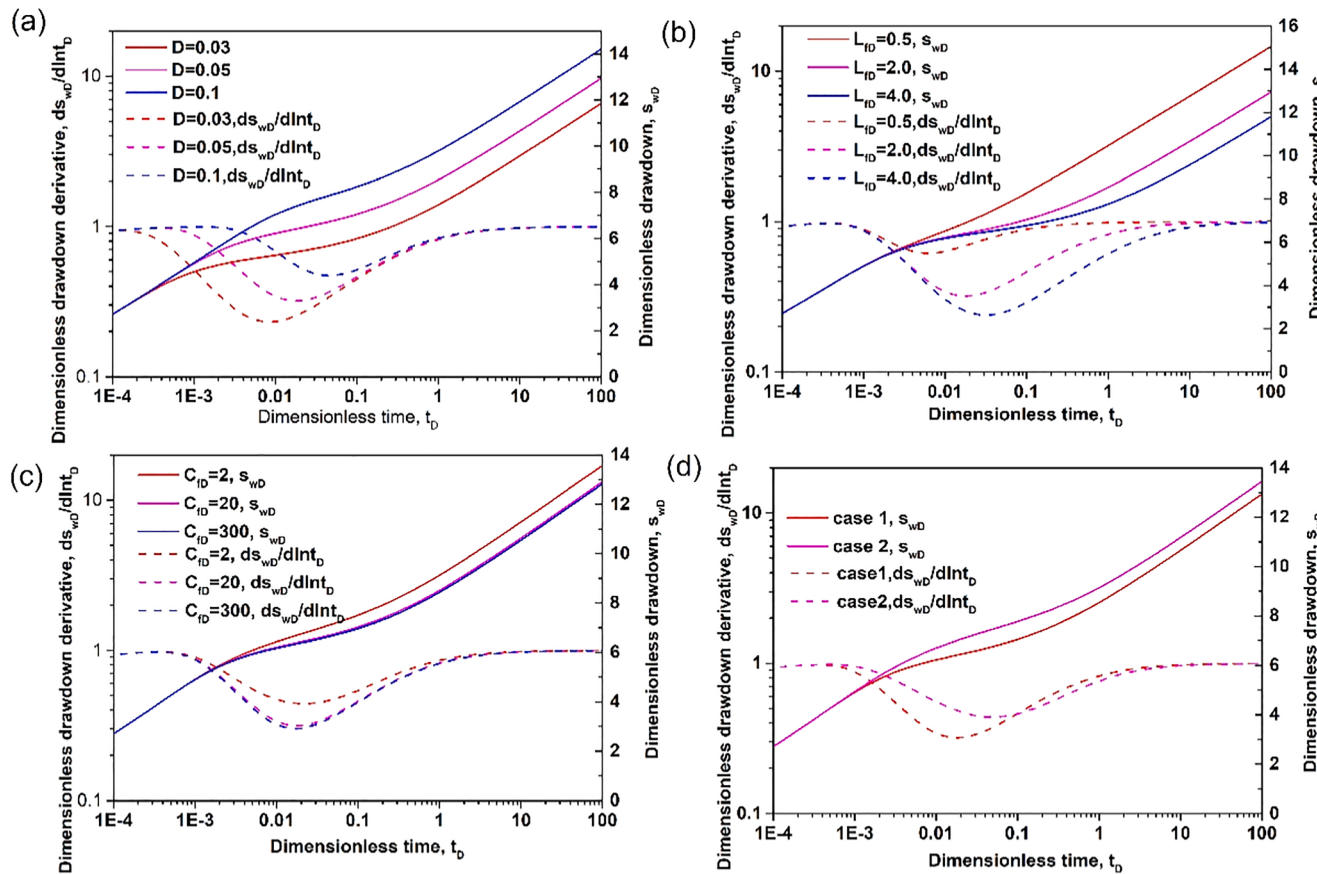


Fig. 6. Dimensionless wellbore drawdown and its derivative versus dimensionless time for a pumping well near a conductive fracture (The solid line represents the drawdown and the dotted line represents the derivative of drawdown). (a) The effect of fracture distance on the drawdown and its derivative for $C_{fd} = 5\pi$ and $L_{fd} = 2$, (b) the effect of fracture length on the drawdown and its derivative for $C_{fd} = 5\pi$ and $D = 0.05$, (c) the effect of fracture conductivity on drawdown and its derivative for $L_{fd} = 2$ and $D = 0.05$, and (d) the effect of fracture location on the drawdown and its derivative for $D = 0.05$ (case 1, the fracture is located at north of the well; case 2, the fracture is located at east of the well).

drawdown vs. time result showed that all drawdown curves coincided with each other in the early time radial flow period; a shorter fracture length yielded a larger drawdown loss in the later period. The plot of the drawdown derivative shows a unit constant straight line in both the early time and later time flow periods, and that a longer fracture length would cause a deeper dip valley in the transient flow period. Fig. 6c

shows the effect of natural fracture conductivity C_{fd} during the drawdown and its derivative. The fracture conductivity C_{fd} was set to 2, 20, and 300, respectively. The distance between a pumping well and a natural fracture D was set to 0.05, and the fracture length L_{fd} was set to 2. The semi-log plot wellbore drawdown vs. time showed that a larger fracture conductivity would cause a smaller drawdown loss; however, this phenomenon was not infinite. When the conductivity is greater than 20, the drawdown loss changes negligibly. The plot of the drawdown derivative shows that a greater conductivity leads to a deeper dip valley. Fig. 6d shows the effect of the relative location between a pumping well and a natural fracture. The fracture length L_{fd} was set to 2. The sub-figure in Fig. 5d shows two cases. The coordinate of a pumping well was located at $(0, 0)$. For case 1, the centre coordinate of the fracture was located at $(0, 0.05)$, and for case 2, the coordinate of fracture's left tip was located at $(0.05, 0)$. The drawdown loss was the largest when the fracture left tip was close to the pumping well, i.e., case 2. The drawdown derivative curve thus implied that case 2 had a shallower dip valley.

3.3. Effect of increasing number of fractures on drawdown behaviour

Fig. 7 shows the effect of a pumping well with additional fractures upon drawdown and its derivative. There are four cases to consider: fracture 1, fractures 1 through 2, fractures 1 through 3, and fractures 1 through 4. Fracture 1 is the nearest to the pumping well. The drawdown derivative plot shows that one dip valley is observed in the transient flow period for case 1 when only fracture 1 is considered. As additional fractures (fractures 2, 3, 4) appear away from the pumping well, a

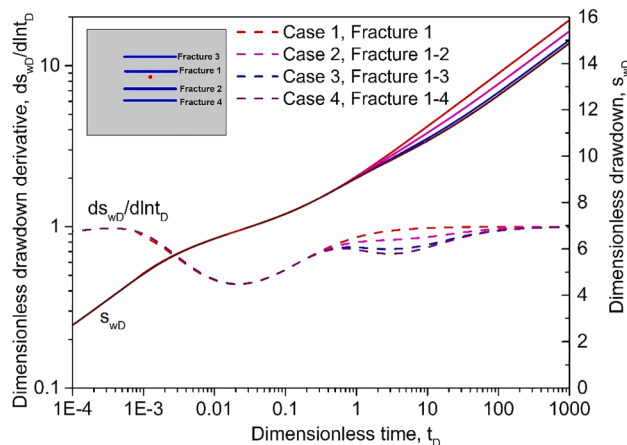


Fig. 7. Effect of the fracture number on the dimensionless drawdown and its derivative for four cases shown in grey subgraph (Case 1, only fracture 1 is considered; case 2, both fracture 1 and fracture 2 are considered; fractures 1 to 3 are considered; fractures 1 to 4 are all considered).

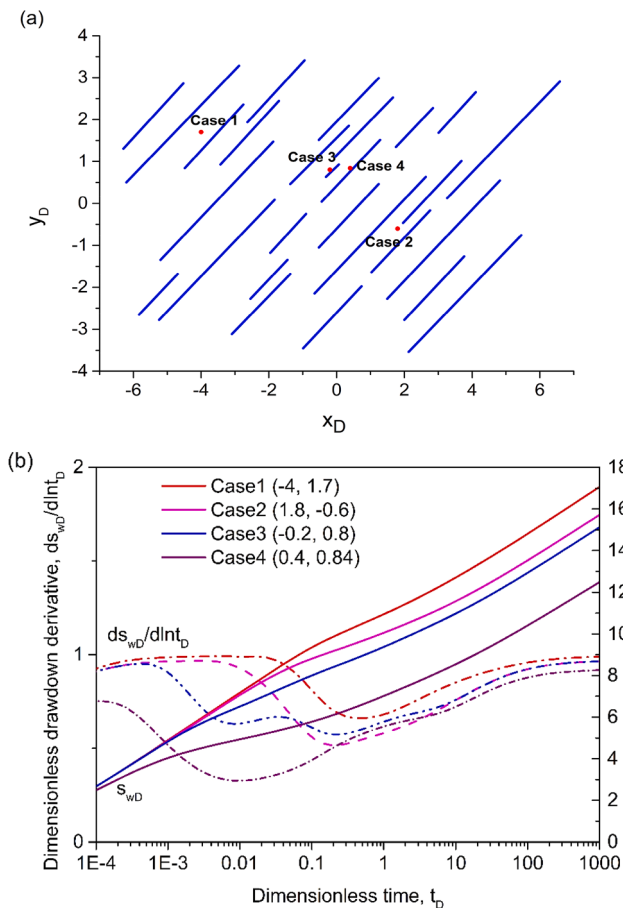


Fig. 8. Effect of the well location on the dimensionless drawdown and its derivative in discretely fractured aquifers with parallel and non-intersected fracture networks. (a) Four well locations (red point) in a random azimuth angle and non-intersected fracture networks and (b) the effect of well location in this situation on the dimensionless drawdown behaviour. (For interpretation of the references to colour in this figure legend, the reader is referred to the web version of this article.)

second dip valley can be found, and the time of occurrence is when the dimensionless time equals 0.3. The first dip valleys for cases 2–4 are in accordance with each other, which also indicates that the first case is mainly affected by fracture 1. There will obviously be additional dip valleys at a certain fracture number, fracture distribution, fracture orientation, fracture length, and fracture width. The drawdown plot shows that when the dimensionless time is less than 0.4, all the curves are coincident with each other, and this implies that 0.4 is the critical point at which other fracture begins to act. When the dimensionless time is more than 0.4, the head loss increases gradually with the increasing natural fractures.

3.4. Effect of well location on drawdown behaviour in fractured aquifers with parallel and non-intersected fracture networks

We have discussed the groundwater drawdown transient behaviour of a pumping well in the vicinity of one fracture and four fractures. Next, we evaluate how the drawdown behaviour of a pumping well's position changes in the fracture networks.

Fig. 8 shows a pumping well arranged in a parallel fracture network with 27 fractures that do not intersect. Fig. 8a shows four well location arrangements to be discussed. In case 1, a pumping well is located at $x_D = -4$ and $y_D = 1.7$, and the pumping well is relatively far away from the fracture. In case 2, a pumping well is located at $x_D = 1.8$ and $y_D = -0.6$, and this well is near a fracture tip. In case 3, a pumping well is located at

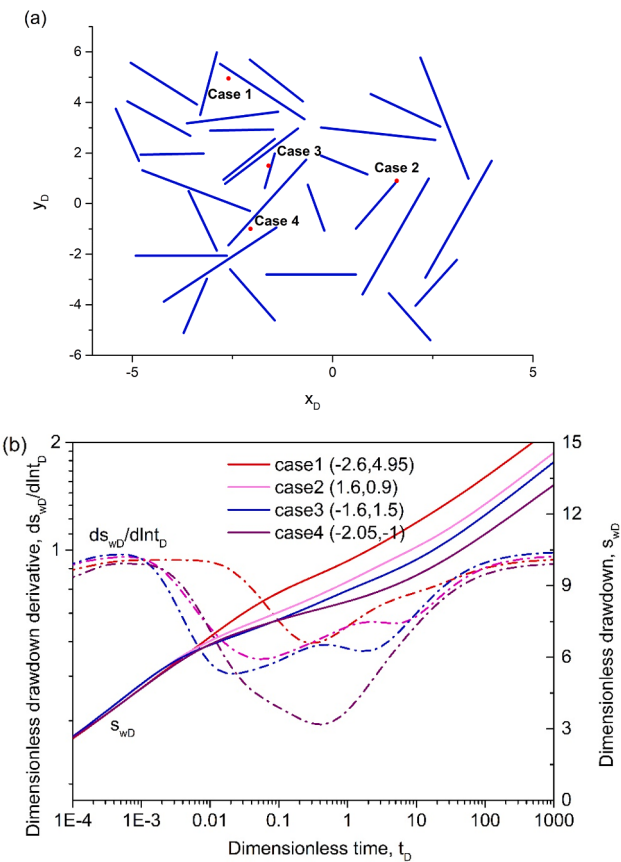


Fig. 9. Effect of the well location on the dimensionless drawdown and its derivative in discretely fractured aquifers with a random azimuth angle and non-intersected fracture networks. (a) Four well locations (red point) in a random azimuth angle and non-intersected fracture networks and (b) the effect of well locations in this situation on the dimensionless drawdown behaviour. (For interpretation of the references to colour in this figure legend, the reader is referred to the web version of this article.)

$x_D = -0.2$ and $y_D = 0.8$, and the pumping well is near a shorter fracture. In case 4, a pumping well is located at $x_D = 0.4$ and $y_D = 0.84$, and the pumping well is near a longer fracture.

Fig. 8b shows the effect of well location on the dimensionless drawdown and its derivative in a parallel and non-intersected fracture network. From the drawdown curve, in case 1, the well is far away from the natural fracture, and the maximum drawdown indicates that the corresponding loss of head is also the largest. In case 4, the pumping well is closest to the longer natural fracture, so its drawdown and loss of head are the smallest. According to these results, we can presume that the loss of head is related to the distances between the well and fracture, fracture conductivity and fracture density, and so on. The derivative curve shows the length of the transient flow period and the number of dip valleys, which are greatly influenced by well location. In case 1, only one dip valley can be observed, and it is shallow and has the shortest duration. In case 2, the pumping well is close to the fracture end point, the duration of transient flow period is relatively long, and the dip valley is deep. In case 3, the pumping well is close to the short fracture and is located in the centre of the fracture network. Three dip valleys can be observed, which is the result of the interaction of natural fractures with different lengths nearby. In case 4, two dip valleys can be observed. Because the well is long, close to the fracture, and located in the centre of the fracture network, the natural fracture has the longest influence time, so the opening of dip valley is exceedingly large.

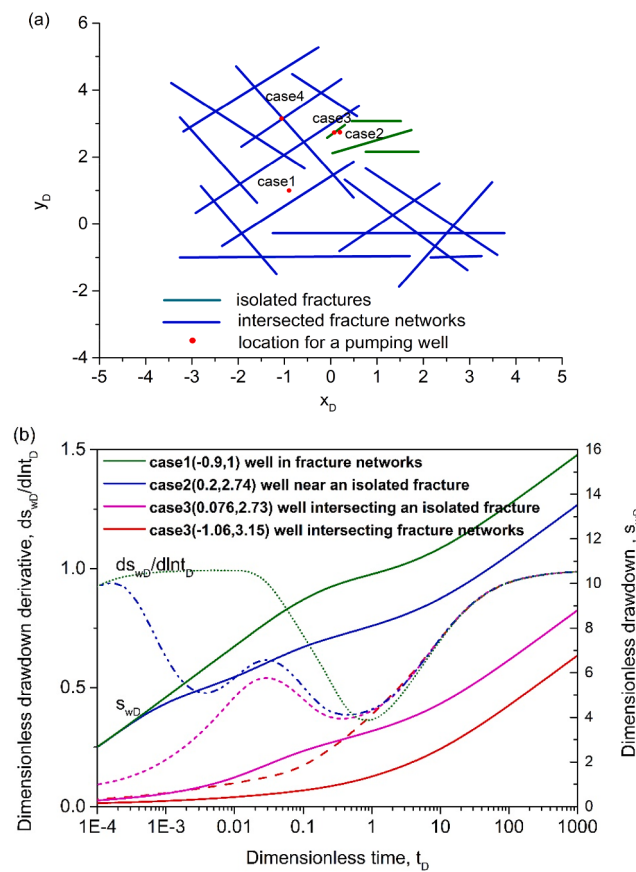


Fig. 10. Effect of the well location on the dimensionless drawdown and its derivative in discretely fractured aquifers with randomly distributed and intersected fracture networks. (a) Four well locations in randomly distributed intersected fracture networks and (b) the effect of well location for a pumping well intersecting or non-intersecting fracture networks.

3.5. Effect of well location on drawdown behaviour in fractured aquifers with a random azimuth angle and non-intersected fracture networks

Fig. 9 shows a pumping well arranged in a fracture network with 30 fractures with random azimuth angles that do not intersect. Fig. 9a shows four well location arrangements to be discussed. In case 1, a pumping well is located at $x_D = -2.6$ and $y_D = 4.95$. A pumping well is positioned at $x_D = 1.6$ and $y_D = 0.9$ in case 2. In case 3, a pumping well is placed at $x_D = -1.6$ and $y_D = 1.5$. In case 4, a pumping well is placed at $x_D = -2.05$ and $y_D = -1$.

The drawdown and drawdown derivative curves are shown in Fig. 9b. In cases 2 and 3, the well location is the closest to the natural fracture. Their associated curves show that the two cases' drawdowns are relatively close. Case 1 shows the maximum drawdown, whereas case 4 contains the minimum drawdown. This indicates that the head loss of the pumping well near the long fracture is the smallest. The drawdown derivative curves also show that only one or two dip valleys are present in each case; moreover, the opening sizes these dip valleys are relatively inconsistent, indicating that the flow behaviour is different under the condition of different well location.

Because the fracture is randomly distributed in the confined aquifers with any angle and any length, the drawdown derivatives of different well positions are strongly unique. One dip valley can be observed in case 1, and two dip valleys can be observed in cases 2 and 3. Owing to the different well locations, there are many possible situations for the shapes of drawdown derivatives; however, this finding is different from the Warren-Root model, which has nothing to do with well locations.

3.6. Effect of well location on drawdown behaviour in fractured aquifers with a random azimuth angle and intersected fracture networks

Unlike previous examples, in the real world, the underground geological conditions are very complex. Under the influence of structure, stress, groundwater environment, dissolution, and other actions, a long-term geological process results in an uneven distribution of natural fractures in the aquifers. Some fractures are connected to form a connected natural fracture network, and some fractures remain isolated and randomly distributed. For a more general example, Fig. 10a shows a pumping well arranged in a complex natural fracture network with 16 intersected fractures (blue lines) and 4 isolated fractures (green lines). Fig. 10a shows four well location arrangements to be discussed. In case 1, a pumping well is placed at $x_D = -0.9$ and $y_D = 1$, where the pumping well is not intersected by fracture networks and is near the intersected fractures. The position of a pumping well in case 2 is $x_D = 0.2$ and $y_D = 2.74$, where the well is near an isolated fracture. In case 3, a pumping well is located at $x_D = 0.076$ and $y_D = 2.73$, where the pumping well intersects an isolated fracture. In case 4, a pumping well is placed at $x_D = -1.06$ and $y_D = 3.15$, and the pumping well is intersected by the connected natural fracture network.

Four cases are shown in Fig. 10b. In cases 1 and 2, when the well does not intersect any fractures, the dimensionless drawdown is higher than the drawdowns in cases 3 and 4. In the early stage, the two drawdown curves coincide with each other. When the dimensionless time is greater than 0.0004, the drawdown curve bifurcates. The dimensionless drawdown of the well arranged in the fracture network is higher than its counterpart, suggesting that the former's head loss is the largest. In cases

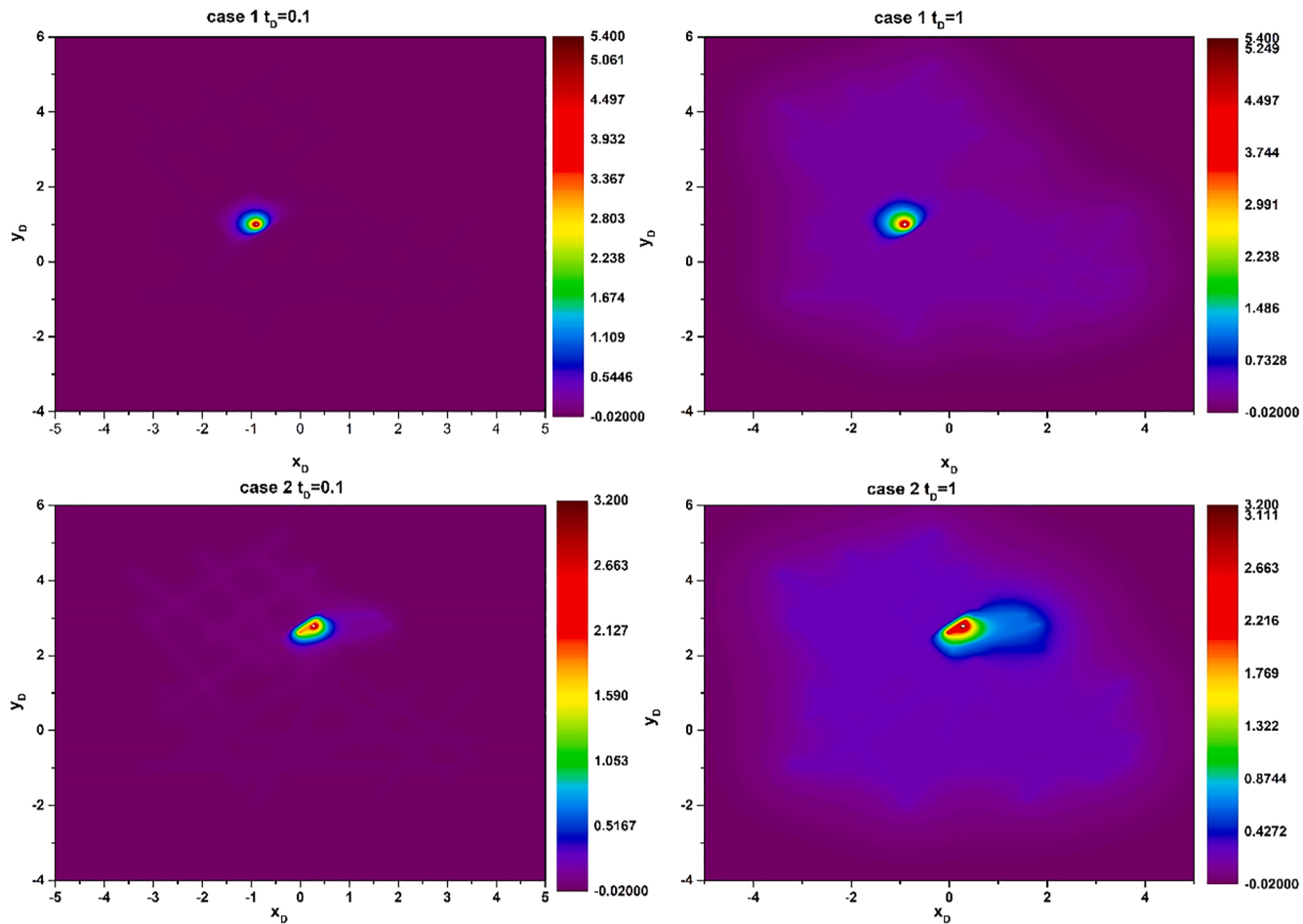


Fig. 11. Effect of well locations on the dimensionless drawdown distribution with intersected fracture networks at for case 1 and case 2: case 1 for the pumping well in the fracture networks ($t_D = 0.1, 1$), and case 2 for the pumping well near an isolated fracture ($t_D = 0.1, 1$).

3 and 4, the drawdown of the well intersecting the fracture is much lower than its counterpart, which implies that the head loss is small when the well is intersected by natural fractures. Finally, the drawdown of the well intersecting the connected fracture network is lower than that of the well intersecting the isolated fracture. The drawdown derivative curve shows that the four cases are considerably different. When a pumping well is arranged in the fracture networks and does not intersect the fracture network, the drawdown derivative curve shows a deep dip valley in the period of unstable flow, which is caused by the influence of the fracture network when the drawdown disturbance propagates to the fracture network. As the isolated fracture is far from the well, it is not felt. In the second case, the isolated fracture closest to the pumping well is felt, and the drawdown derivative shows the first dip valley. Then, as the drawdown disturbance continues to propagate, the connected fracture network is sensed, and the second dip valley appears. Because of the large area of the fracture network connected by large fractures, the second dip valley is deeper. In the third case, when a well is crossed by an isolated fracture, only a single dip valley can be observed because the fracture network is felt. At this time, the pumping well and the isolated fracture are connected as a whole. In the fourth case, the pumping well is crossed by the connected fracture network, and no dip valley is felt because the whole fracture network and the well are considered as a whole.

Figs. 11 and 12 show the drawdown field distribution at the dimensionless time $t_D = 0.1$. The drawdown in case 1 is the largest because the pumping well is in the matrix and is far away from the fracture, and the wellbore drawdown has no place to release. The lowest head loss is in case 4. When the well is connected with the connected

fracture network, because the propagation speed of the fracture network is rapid, the drawdown quickly affects the entire fracture network. The drawdown in case 2 is similar to that in case 3. The well is near or intersects with the isolated fracture, and the head loss is also large. This is because the isolated fracture is not connected with the fracture network, and its propagation speed is affected by the low hydraulic conductivity in matrix. Figs. 11 and 12 intuitively demonstrate the evolution of head contours over time in different cases of fracture configurations. The drawdown increases with time, and the flow characteristic on wellbore is determined by the pattern of the head contour.

In the conventional Warren-Root model and traditional concept (Warren and Root, 1963; Moench, 1984; Hamm and Bidaux, 1996; Lods and Gouze, 2004), the shape of the dip valley is mainly affected by two factors: the storage coefficient and the inter-porosity coefficient. However, this study illustrates that the number of dip valleys on the curve of drawdown derivative is closely related to the fracture density, fracture length, fracture conductivity, fracture distribution, and position of the well.

4. Conclusions

This study proposed a novel semi-analytical model to study the drawdown transient behaviour in a fractured aquifer with multiple intersecting or isolated natural fractures. Aquifer and natural fracture models were both established. The coupling model and linear equations were obtained through the coupling conditions of fracture wall in Laplace space. The final drawdown solution was proposed using the Stehfest numerical inversion. The following conclusions were derived:

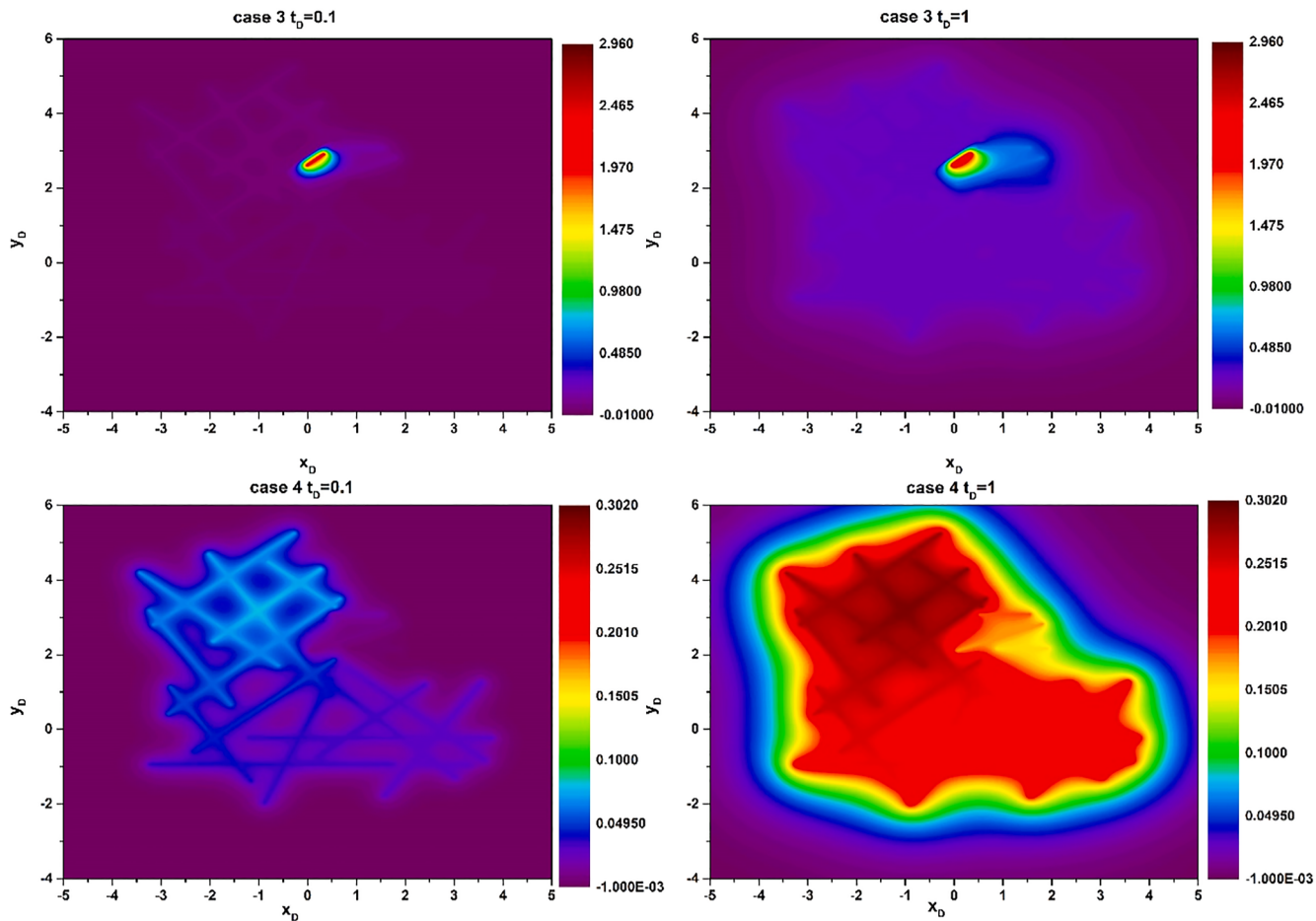


Fig. 12. Effect of well locations on the dimensionless drawdown distribution with intersected fracture networks at for case 3 and case 4: case 3 for the pumping well intersecting an isolated fracture ($t_D = 0.1, 1$), and case 4 for the pumping well intersecting fracture networks ($t_D = 0.1, 1$).

- (1) The presented drawdown solution was compared with a previous solution for a pumping well intersected by a natural fracture with double wings, and the comparative results were in accordance.
- (2) The case for a pumping well with an isolated fracture showed the important effects of fracture conductivity, fracture length, distance between the well and fracture, and location of the fracture during dimensionless drawdown.
- (3) The case for a pumping well with four isolated fractures showed that the drawdown derivative was obviously affected by the fracture number. Additional dip valleys will occur with an increasing fracture number, and the head loss increased gradually with the increasing natural fractures.
- (4) The effect of well location on drawdown behaviour in fractured aquifers with parallel and non-intersected fracture networks was analysed. The result indicated that because the studied well was long, close to the fracture, and placed at the centre of the isolated fracture network, the natural fracture had the longest influence time, so the dip valley opening was large. Three dip valleys were observed, which was the result of the interaction of natural fractures with different lengths.
- (5) The effect of well location on the drawdown behaviour in fractured aquifers with random azimuth angles and non-intersected fracture networks was evaluated. The head loss of the pumping well near the long fracture was the smallest. Moreover, the calculation results showed that when the pumping well was intersected by the connected fracture network, the head loss was the smallest. During the pumping test process, the well should be drilled into the connected fracture network as much as possible.

CRediT authorship contribution statement

Lei Wang: Conceptualization, Writing - original draft. **Hong Zhou:** Data curation, Validation. **Junlei Wang:** Methodology. **Rongze Yu:** Writing - review & editing. **Jianchao Cai:** Supervision.

Declaration of Competing Interest

The authors declare that they have no known competing financial interests or personal relationships that could have appeared to influence the work reported in this paper.

Acknowledgements

This work is supported by the National Natural Science Foundation of China (No. 41722403 and 51804284), the Fundamental Research Funds for the Central Universities, China University of Geosciences (Wuhan) (Nos. 162301182780 and CUGGC04), and the National Science and Technology Major Project Foundation of China (grant no.2017ZX05035-004-005). We declare that we have no conflict of interest.

Appendix A. Supplementary data

Supplementary data to this article can be found online at <https://doi.org/10.1016/j.jhydrol.2020.125737>.

References

- Bourdet, D., Whittle, T.M., Douglas, A.A., et al., 1983. A new set of type curves simplifies well test analysis. *World Oil*. 96 (6), 95–106.
- Barenblatt, G.E., Zheltov, I.P., Kochina, I.N., 1960. Basis concepts in the theory of seepage of homogeneous liquids in fissured rocks. *J. Appl. Math. Mech. Engl. Transl.* 24 (5), 1286–1303.
- Batu, V., 1998. *Aquifer Hydraulics: A Comprehensive Guide to Hydrogeologic Data Analysis*. John Wiley & Sons Inc, New York.
- Boulton, N.S., Streltsova, T.D., 1977. Unsteady flow to a pumped well in a fissured water-bearing formation. *J. Hydrol.* 35, 257–269.
- Cai, J., Wei, W., Hu, X., et al., 2017. Fractal characterization of dynamic fracture network extension in porous media. *Fractals* 25 (2), 1750023.
- Chen, Z.M., Liao, X.W., Zhao, X.L., et al., 2016. A semianalytical approach for obtaining type curves of multiple-fractured horizontal wells with secondary-fracture networks. *SPE J* 21 (2), 538–549.
- Cheng, A.-H.-D., 2000. *Multilayered Aquifer Systems—Fundamentals and Applications*. Marcel Dekker, New York/Basel.
- Cinco-Ley, H., Meng, H.-Z., 1988. Pressure transient analysis of wells with finite conductivity vertical fractures in double porosity reservoirs. *SPE Annual Technical Conference and Exhibition*, 2–5 October, Houston, Texas, SPE-18172-MS.
- Ge, S., 1997. A governing equation for fluid flow in rough fractures. *Water Resour. Res.* 33 (1), 53–61.
- Gerke, H.H., van Genuchten, M.T., 1993. A dual-porosity model for simulating the preferential movement of water and solutes in structured porous media. *Water Resour. Res.* 29 (2), 305–319.
- Gringarten, A.C., Ramey, H.J., Raghavan, R., 1974. Unsteady-state pressure distributions created by a well with a single infinite-conductivity vertical fracture. *Soc. Pet. Eng. J.* 14 (4), 347–360.
- Hamm, S., Bidaux, P., 1996. Dual-porosity fractal models for transient flow analysis in fissured rocks. *Water Resour. Res.* 32 (9), 2733–2745.
- Jenkins, D.N., Prentice, J.K., 1982. Theory for aquifer test analysis in fractured rocks under linear (nonradial) flow conditions. *Groundwater* 20 (1), 12–21.
- Kazemi, H., 1969. Pressure transient analysis of naturally fractured reservoirs with uniform fracture distributions. *Trans. Soc. Pet. Eng.* 246, 451–462.
- Karimi, M.F., Durlofsky, L.J., Aziz, K., 2004. An efficient discrete-fracture model applicable for general-purpose reservoir simulators. *SPE J* 9 (2), 227–236.
- Kruseman, G.P., de Ridder, N.A., 1991. Analysis and evaluation of pumping test data. Wageningen, International Institute for Land Reclamation and Improvement Publication, p. 47.
- Kuhlman, Kristopher L., 2013. Review of inverse Laplace transform algorithms for Laplace-space numerical approaches. *Numer. Algorithms* 63(2), 339–355.
- Kuhlman, K.L., Neuman, S.P., 2009. Laplace-transform analytic-element method for transient porous-media flow. *J. Eng. Math.* 64 (2), 113–130.
- Lods, G., Gouze, P., 2004. WTFM, software for well test analysis in fractured media combining fractional flow with double porosity and leakance approaches. *Comput. Geosci.* 30 (9–10), 937–947.
- Lee, S.H., Lough, M.F., Jensen, L.C., 2001. Hierarchical modeling of flow in naturally fractured formations with multiple length scales. *Water Resour. Res.* 37 (3), 443–455.
- Liu, R., Jiang, Y., Huang, N., et al., 2018. Hydraulic properties of 3D crossed rock fractures by considering anisotropic aperture distributions. *Adv. Geo-Energy Res.* 2 (2), 113–121.
- Luo, W.J., Tang, C.F., Zhou, Y.F., 2019. A new fracture unit model and its application to a Z fold fracture. *SPE J.* 24 (1), 319–333.
- Mei, L., Zhang, H., Wang, L., et al., 2020. Fractal analysis of shape factor for matrix-fracture transfer function in fractured reservoirs. *Oil Gas Sci. Technol.–Revue d'IFP Energies nouvelles* 75, 47.
- Moench, A.F., 1984. Double-porosity models for a fissured groundwater reservoir with fracture skin. *Water Resour. Res.* 20 (7), 831–846.
- Nielsen, K.A., 2007. *Fractured Aquifers—Formation Evaluation by Well Testing*. Trafford Publishing, Canada.
- Önder, H., 1998. One-dimensional transient flow in a finite fractured aquifer system. *Hydrol. Sci. J.* 43 (2), 243–265.
- Olorode, O., Freeman, C.M., Moridis, G., et al., 2013. High-resolution numerical modeling of complex and irregular fracture patterns in shale-gas reservoirs and tight gas reservoirs. *SPE Res. Eval. Eng.* 16 (4), 443–455.
- Qiu, F., Porcu, M.M., Xu, J., et al., 2015. Simulation study of zipper fracturing using an unconventional fracture model. *SPE/CSUR Unconventional Resources Conference*, 20–22 October, Calgary, Alberta, Canada, SPE-175980-MS.
- Sen, Z., 1986. Aquifer test analysis in fractured rocks with linear flow pattern. *Groundwater* 404 (1), 72–76.
- Strack, O.D.L., 1989. *Groundwater Mechanics*. Prentice-Hall, New York.
- Stehfest, H., 1970. Numerical inversion of Laplace transforms. *Commun ACM* 13 (1), 47–49.
- Slimani, K., Tiab, D., 2008. Pressure transient analysis of partially penetrating wells in a naturally fractured reservoir. *J. Can. Pet. Technol.* 47 (5), 63–69.
- Smedt, F.D., 2011. Analytical solution for constant-rate pumping test in fissured porous media with double-porosity behaviour. *Transp Porous Media* 88, 479–489.
- Wang, L., Dai, C., Xue, L., 2018a. A semi-analytical model for pumping tests in finite heterogeneous confined aquifers with arbitrarily shaped boundary. *Water Resour. Res.* 54 (4), 3207–3216.
- Wang, J.L., Jia, A.L., Wei, Y.S., 2018b. A general framework model for simulating transient response of a well with complex fracture network by use of source and Green's function. *J. Nat. Gas Sci. Eng.* 55, 254–275.
- Warren, J.E., Root, P.J., 1963. The behavior of naturally fractured reservoirs. *SPE J.* 3 (2), 245–255.
- Walton, W.C., 2006. *Aquifer Test Modelling*. CRC Press, Taylor & Francis Group, Boca Raton.
- Xu, Y., Cavalcante Filho, J.S.A., Yu, W., et al., 2017. Discrete-fracture modeling of complex hydraulic-fracture geometries in reservoir simulators. *SPE Res. Eval. Eng.* 20 (2), 403–422.
- Zeng, F.H., 2008. Modeling of non-Darcy flow in porous media and its application. PhD Thesis. University of Regina.